scientific reports

Check for updates

OPEN

Adsorption and bacterial performance of Nd_2O_3 modified Ag nanoparticles with enhanced degradation of methylene blue

Mohamed Tharwat Elabbasy[1], M. A. El-Morsy[2,3], Nasser S. Awwad[4], Hala A. Ibrahium[5] & A. A. Menazea[6]✉

Our study focused on the optical behavior, methylene blue (MB) dye degradation potential, antibacterial performance, and silver and trioxide mineral interaction with different bacterial species. We found that the addition of silver nanoparticles (Ag NPs) to neodymium oxide (Nd_2O_3) resulted in a significant response, with an enlargement of the inhibition zone for bacterial species such as *Staphylococcus aureus* and *Escherichia coli*. Specifically, the inhibition zone for *S. aureus* increased from 9.3 ± 0.5 mm for pure Nd_2O_3 to 16.7 ± 0.4 mm for the Ag/Nd_2O_3 nano-composite, while for *E. coli*, it increased from 8.8 ± 0.4 mm for Nd_2O_3 to 15.9 ± 0.3 mm for Ag/Nd_2O_3. Furthermore, the optical behavior of the composites showed a clear band-gap narrowing with the addition of Ag NPs, resulting in enhanced electronic localization. The direct and indirect transitions reduced from 6.7 to 6.1 eV and from 5.2 to 2.9 eV, respectively. Overall, these results suggest that the Ag/Nd_2O_3 nano-composite has potential applications in sensor industries and water treatment, thanks to its enhanced optical behavior, antibacterial performance, and efficient MB degradation capabilities. In terms of MB degradation, the Ag/Nd_2O_3 mixed system exhibited more efficient degradation compared to pure Nd_2O_3. After 150 min, the MB concentration in the mixed system decreased to almost half of its starting point, while pure Nd_2O_3 only reached 33%.

Keywords Optical, Silver nanoparticles, Neodymium oxide, Water treatment

In the modern domain, the routine usages of cosmetics, dyes, and chemicals are amplified. Thus, global water resources were contaminated via leftover chemicals and dyes. This contamination directly affected all living creatures[1–6]. The existence of dye in water is toxic, and also prevent sunlight passing through water which influences aquatic organisms. Henceforth, appropriate dye removal is essential before its release to water bodies. decomposition of dye pollutants into non-toxic ingredients is a challenge[7]. Advanced Oxidation Processes (AOPs) for removing pollutants embrace several methods, for instance, ozonation, photocatalysis, and electrochemical oxidation. In this study Methylene blue (MB) dye was decomposed upon Ag/Nd_2O_3 utilization. The MB dye contamination is spread widely owing to its usage in dyeing and printing textile industries[8]. The azo functional group (–N=N–) which exists in MB structure is considered carcinogenic[9]. Additionally, methylene blue (MB) inhalation affects digestive system pains, respiratory system sicknesses, as well nervous systems disorders[10]. Saravanan et al.[11] develop a dye removal Photocatalytic process by replacing UV radiation instead with visible electromagnetic waves. Photocatalytic degradation is influenced by band-gap, surface area, and grain size, and amount of material[12]. Metallic nano-scale metals possess special physical and chemical activity that push in exploiting them in numerous fields such as electronics, textile, medical, etc. catalytic potential of metals recommends its usage in the degradation of toxic dyes[7]. Further, metallic insertions belong to exceptional electric, magnetic and optical performances. Semiconductor catalysts are preferred in the process of photocatalytic degradation of

[1]Pathology Department, College of Medicine, Ha'il University, 55476 Ha'il, Saudi Arabia. [2]Physics Department, Plasma Technology and Material Science Unit, College of Science and Humanities in Al-Kharj, Prince Sattam Bin Abdulaziz University, 11942 Al-Kharj, Saudi Arabia. [3]Physics Department, Faculty of Science, University of Damietta, New Damietta 34517, Egypt. [4]Department of Chemistry, College of Science, King Khalid University, P.O. Box 9004, 61413 Abha, Saudi Arabia. [5]Department of Biology, College of Science, King Khalid University, P.O. Box 9004, 61413 Abha, Saudi Arabia. [6]Spectroscopy Department, Physics Research Institute, National Research Centre, Dokki 12622, Giza, Egypt. ✉email: aanter7@gmail.com

wastewater due to several advantages. Firstly, they are cost-effective. Secondly, they are non-toxic. Thirdly, they possess adaptable characterization that could be altered through doping, size adjustment, or sensitizers. Fourthly, they enable a multi-electron relocation process. Lastly, they can be utilized extensively without significant reduction in their photocatalytic efficiency[13].

The optical and magnetic characteristics of Neodymium oxide nanoparticles have much attention for numerous usages. Indeed, Nd_2O_3 is extensively utilized in photonic, luminescent, and thermo luminescent usages[9]. Moreover, grayish blue hexagonal crystal lattice of neodymium oxide (Nd_2O_3) offers significant catalytic, electric, coloring, besides additive characteristics[14,15]. Nd_2O_3 enhances photocatalytic activity by facilitating the effective separation of photo-generated electrons[16]. Casillas et al.[17], studied the photo-catalytic degradation of diclofenac in aqueous system catalyzed with Al_2O_3–Nd_2O_3 oxides and the effectiveness linked to the Nd_2O_3 contribution. Studying silver doped neodymium oxide nano-composite is favored owing to its inertness, non-toxicity, high surface area[10], which are different from their macro-scaled equivalents. Additionally, the energy gap could be narrowed by modifying surface defects by forming nano-composites[17]. A research revealed that CuO nanoparticles doped with Nd_2O_3 had a remarkable photocatalytic efficacy, reaching up to 90.8% during a duration of 80 min, accompanied with a degradation rate of 0.0227 min^{-1}[18]. On the other hand, from 90 to 100% degradation was detected for several dyes by silver NPs. Also, the advantage of NPs usage in dye degradation process is time saving with lacking any hazardous chemical[7]. Such usages strongly depend on the morphological features, and crystal structure of silver NPs[19]. The incorporation of AgNPs into Nd_2O_3 improves the efficiency of photocatalysis due to many factors. To begin with, doping involves the incorporation of distinct metallic elements into the structure of the photocatalyst, resulting in a fundamental modification of its physical and chemical characteristics. This allows for the inclusion of a larger quantity of photogenerated electrons and holes, so effectively adjusting the reaction towards visible wavelengths[20]. Furthermore, AgNPs enhance the photocatalytic activity driven by ultraviolet light by facilitating the separation of electrons and holes. Additionally, AgNPs also stimulate the photocatalytic activity driven by visible light via the localized surface plasma resonance (LSPR) of AgNPs[20]. Hence, the addition of AgNPs to Nd_2O_3 doping might augment the photocatalytic efficiency by broadening the spectrum of light absorption and facilitating the segregation of photo-generated charge carriers[20,21]. Further, the plasmon excitation boosts optical field response[19]. Lately scientists notify AgNPs as a recommended degradation agent of methylene blue[7]. Owing to the previous survey; Nd_2O_3, and Ag NPs are recommended for effective dye removal strategy. The microstructure, optical, and antibacterial behavior is examined.

Bacteria, fungus, and plants are effectively used in biological methods to degrade different textile dyes. In order to harness the capabilities of microbial consortia for improving dye degradation, it is important to consider the wide range of enzyme activation that might occur within a culture. The drawbacks of this approach include the need for prolonged retention times for the conversion of a functional molecule and its complete mineralization. The combination of photocatalysis for dye removal and antibacterial activity for water treatment is more effective and will reduce the cost of the water treatment process[22].

The objective of this paper is to illustrate the influence of Photocatalytic properties on the dyes removal capability and assess the adsorption aptitude of Nd_2O_3 and AgNPs compositions in environmental applications, particularly water decontamination and antibacterial activity. Additionally, the research aims to examine the optical behavior of the pure Nd_2O_3 composition.

Experimental techniques

Preparation of Ag/Nd_2O_3 NPs

In the first step, 100.0 mL of 0.1 M silver nitrate (99.9%) was mixed by 100.0 mL of 0.1 M neodymium chloride (99.8%) solution. In the second step, 200 mL of 0.1 M thio-urea solution has been added while manipulating the temperature at 80 °C for 3 h on a magnetic stirrer. Throughout the heating process, 1 M NaOH (99%) has been gradually added to obtain the desired alkaline precipitate. After 3 h, the mixture was cooled down to room temperature and then washed with distilled water and ethanol to dissolve any contaminations. Finally, the precipitate was dried at 70 °C for three days. During the stirring and heating process, the following reactions were predicted: Sodium hydroxide was dissolved, giving aqueous sodium cations and hydroxyl anions, as well as silver nitrate and neodymium chloride[13]. The following equations were predicted.

$$OH^-_{(aq)} + Nd^{3+}_{(aq)} + Ag^+_{(aq)} \rightarrow AgOH_{(aq)} + Nd(OH)_{3(aq)}$$

$$AgOH_{(aq)} + Nd(OH)_{3(aq)} \rightarrow Ag/Nd_2O_{3(s)} \downarrow + 2H_2O$$

The resultant product is not water soluble as Nd_2O_3 has a very low solubility in water[23,24].

All raw chemicals have been obtained from Sigma Aldrich. The powder of Ag/Nd_2O_3 NPs was exposed to UV–Vis spectroscopy analysis (Lamda-950, PerkinElmer, Germany). The X-ray diffraction (XRD) pattern was attained by an X-ray diffractometer (XRD, X'Pert Explorer, PANalytical diffractometer) equipped with Cu Kα1 radiation (λ = 1.5406 nm) utilizing a originator voltage of 40 kV and current of 35 mA. FTIR analysis have been executed with a spectrometer (iS50 ATR Spectrum-100 FTIR) gotten from PerkinElmer, Germany. High resolution transmission electron microscope (HRTEM, JEM-2100F) has been utilized for the synthesized samples. Additionally, MB degradation evaluation was executed by a spectrophotometer[24].

The concentration of methylene blue (MB) solution was modified to 20 ppm and the pH was 6. The lighting system used a closed box to emit visible light within the spectrum of 500 watts. Following irradiation, a volume of 3 mL was extracted from the (MB) solution at certain time intervals for analysis using a spectrophotometer. The deterioration potential is determined using the mathematical formula[25,26]. Following the degradation of MB, the resulting precipitated powder was subjected to centrifugation for the purpose of recycling[27,28].

Preparation of Bacterial Culture: A bacterial culture is created by cultivating bacteria in a media that is abundant in nutrients, hence facilitating their development and multiplication. The culture is placed in a controlled environment to facilitate bacterial growth. Following the incubation period, the culture is examined. If the antibacterial treatment is effective, there should be a region where bacterial proliferation is impeded. The antibacterial activity may be quantified by measuring and using this zone. The antibacterial activity has been tested against both Gram-negative (*Escherichia coli* = *E. coli*) and Gram-positive (*Staphylococcus aureus* = *S. aureus*). The experiment begun with 5 mg/ml starting concentration for the synthesized samples to be examined. The inhibition zone has been measured after 24 h of incubation at 37 °C under visible light.

Discussion

XRD

Crystallinity was clarified by XRD analysis that 2θ were introduced in 10–70 scope. For silver, the bands were confirmed its existing, utilizing JCPDS no. 04-0783. Various peaks for silver attained at $2\theta = 38.3°$, 43.9°, 65.1°, and 77.3°, which corresponds to the Bragg's reflections of the (111), (200), (220), and (311) crystal planes of the face-centered cubic (fcc) structure of metallic silver[29]. Figure 1 also marks peaks for Nd_2O_3 according to JCPDS no. 21-0579[30]. The peaks of Nd_2O_3 which are at $2\theta = 27.8$, 29°, 40.2°, 49°, 51.6, and 57° ,can be indexed to the (100), (002), (102), (110), (103), and (112), respectively[31]. The resultant patterns do not refer to any major disorders owing to the silver nanoparticle's contribution[17].

FTIR

The FTIR spectra are revealed in Fig. 2. It can be observed that the broadband at 3455 cm^{-1} for pure oxide while adding silver NPs does not cause a noticeable shift that O–H stretching vibration of the –OH group appears at 3448 cm^{-1}[32]. The revealing absorption peak at 3554 cm^{-1} is assigned to thio-urea residual N–H stretching[33]. The Neodymium oxide (Nd_2O_3) NPs strong band centered at 669 cm^{-1} is attributed to Nd–OH which shows significant diminishing with adding Silver nano-particles[32]. The centered bands at 588 cm^{-1} was because of –O stretching of Nd[30]. The previously mentioned bands confirm Nd_2O_3, Ag/Nd_2O_3 chemical composition.

TEM

Nd_2O_3 NPs microstructure is demonstrated in Fig. 3a. Distinct grains for pure Neodymium oxide are appeared, while Silver nanoparticles appeared with well-defined grains upon the Nd_2O_3 matrix. Silver nano-particles average grain size is 9.2 nm. As well, Nd_2O_3 introduces significant crystalline portions with distinct grain borders. In addition, the circle inserted in the same figure displays fringes of diffraction points; thus, the presence of well-crystallized Neodymium oxide is approved[17]. The displayed Fig. 3b micrograph confirms the good distribution of Ag NPs upon Nd_2O_3, besides the well matching with XRD results. The red circles represent AgNPs which is inside the surface of Nd_2O_3 which is represented in blue circles. Figure 3c represent saed pattern for Ag/Nd_2O_3NPs and Fig. 3d obtained the particle size histogram of Ag/Nd_2O_3NPs.

Optical study

Studying the optical characteristics of nano-composite have an excessive curiosity in order to discover their proper usage. The optical characteristics of Nd_2O_3 and Ag/Nd_2O_3 nanoparticles were inspected by UV–Vis spectroscopy in wavelengths ranging from 200 to 1100 nm. The band at 244 nm is for Nd_2O_3 NPs that allied an interchange of electrons among the valence and conduction orbits[32]. The optical band gap energy has been assessed by mode suggested by Wood and Tauc. Aiming for optically induced transition understanding, optical

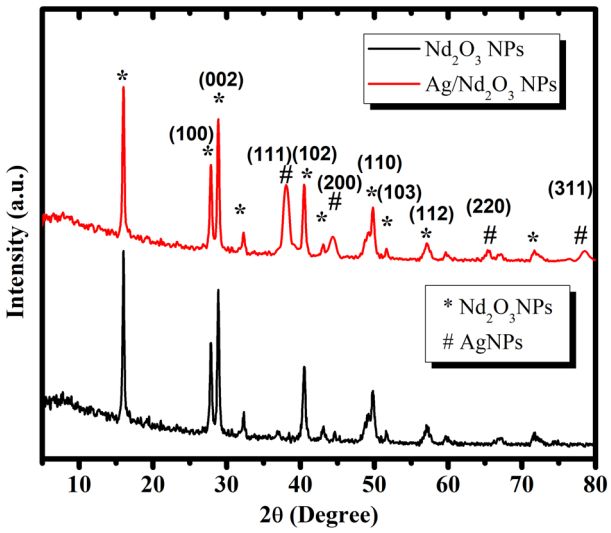

Figure 1. XRD of Pure Nd_2O_3 NPs, and Ag/Nd_2O_3NPs.

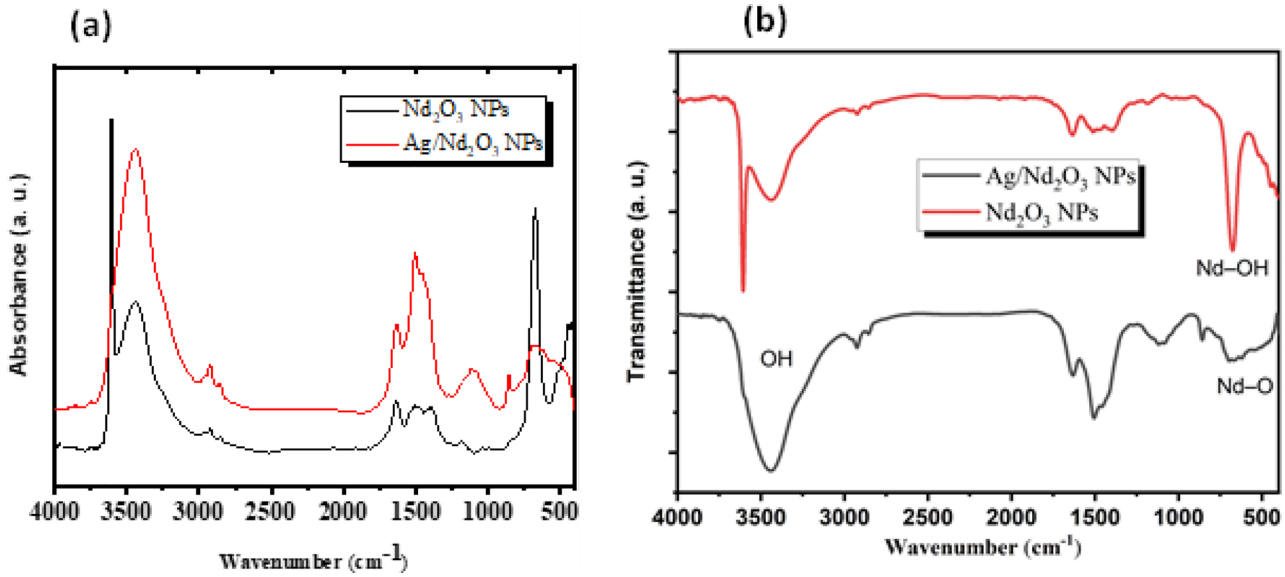

Figure 2. FTIR of Pure Nd_2O_3 NPs, and Ag/Nd_2O_3NPs.

band-gaps are obtained from UV absorption spectra. The technique is based on the absorption of a relatively high energetic photon in comparison to bandgap energy. Briefly, there are two types of optical transitions based on absorption edge, they are direct and indirect transitions. Both transition types involve an interaction of the valence band with an electromagnetic wave.

The Optical absorption coefficient (α) is calculated by Beer–Lambert's equation[34]. After that, the absorption coefficients (α) plot against (hν) in Fig. 4, showing absorption edge shift was obtained due to silver assimilation. The Eg values were almost 6.8 e.V for pure Neodymium oxide (Nd_2O_3) NPs[32]. On the other hand, Ag NPs insertion causes shifting of λ to lower frequency[35], besides lowering absorption edge to 6.1 e.V[30]. this confirms the well spreading of silver NPs[36]. As well, the band-gap is estimated from $\alpha h\nu = A(h\nu - Eg)^m$ equation[37,38], where (hν) is for photon energy, (Eg) is for band-gap, (A) is for band tailing parameter, and (m) direct transition is at m = 0.5, and indirect transition is at m = 2).

Bandgap widened with size shrinkage owing to electron confinement at nano-scale which is famed for the "quantum size effect". The diminishing of bandgap refers to the perfection in crystallographic ordering by adding Ag NPs that enhance boosting in electronic localization upon nano-composite ingredients[39,40]. Consequently, these interpretations boost these compositions' usage in sensors industries.

Finally, The refractive index (n) is computed using Dimitrov and Sakka formula as a function of indirect energy band-gap.

$$\frac{n^2-1}{n^2+1} = 1 - \sqrt{\frac{Eg_i}{20}} \tag{1}$$

In likewise, addition, the refractive index alteration as listed in Table 1 refers to varying packing density[36]. This specifies Nd_2O_3 NPs and Ag/Nd_2O_3 NPs to be utilized in optoelectronic devices.

Methylene blue (MB) degradation assessment by Uv–Vis Absorption Analysis

The characteristic absorbance peak of methylene blue dye was centered at 618 nm. Throughout the irradiation step, the crest in both cases (Nd_2O_3 and Ag/Nd_2O_3) shows a regular decline in absorbance owing to hypochromic influence. The absorbance of MB solution shows a dwindling pattern with time. this could explain the adsorbing capability of both tested compositions, However, the silver-containing composition exhibits a higher potential for degradation[41]. This may be explained by Nd_2O_3 capability to absorb photons that enhance electron excitation, generating positive holes. The electron–hole pairs travel individually to the surface of oxide and lead to redox series with adsorbed species, generating highly reactive oxygen species (ROS). These oxy-species interact with adsorbed contaminations leading to the decomposition process[42]. However, after short time electrons and holes recombine causing a decline in its photo-degradation potential. Thus, decreasing their recombination is executed by metals that act as cationic dopants[42]. Further, in this study degradation assessment of pure Nd_2O_3 and $AgNd_2O_3$ nanoparticles Mixed System is executed under visible light. Spectra display a gradual dropping of MB content with irradiation time. The MB degradation efficiency is detected via λ_{max} peak intensity, thus the dye concentration shows a declining pattern with the time that confirms its efficiency in removing the MB dye. Mixed System shows more efficient degradation owing to silver nano-particle insertion that the MB concentration dropped to half of its starting point at 150 min. Also, The photo-conversion capability using pure Nd_2O_3 as a reference photo-catalyst was lower than those of nano-composite, reaching 33% after 150 min of light irradiation,

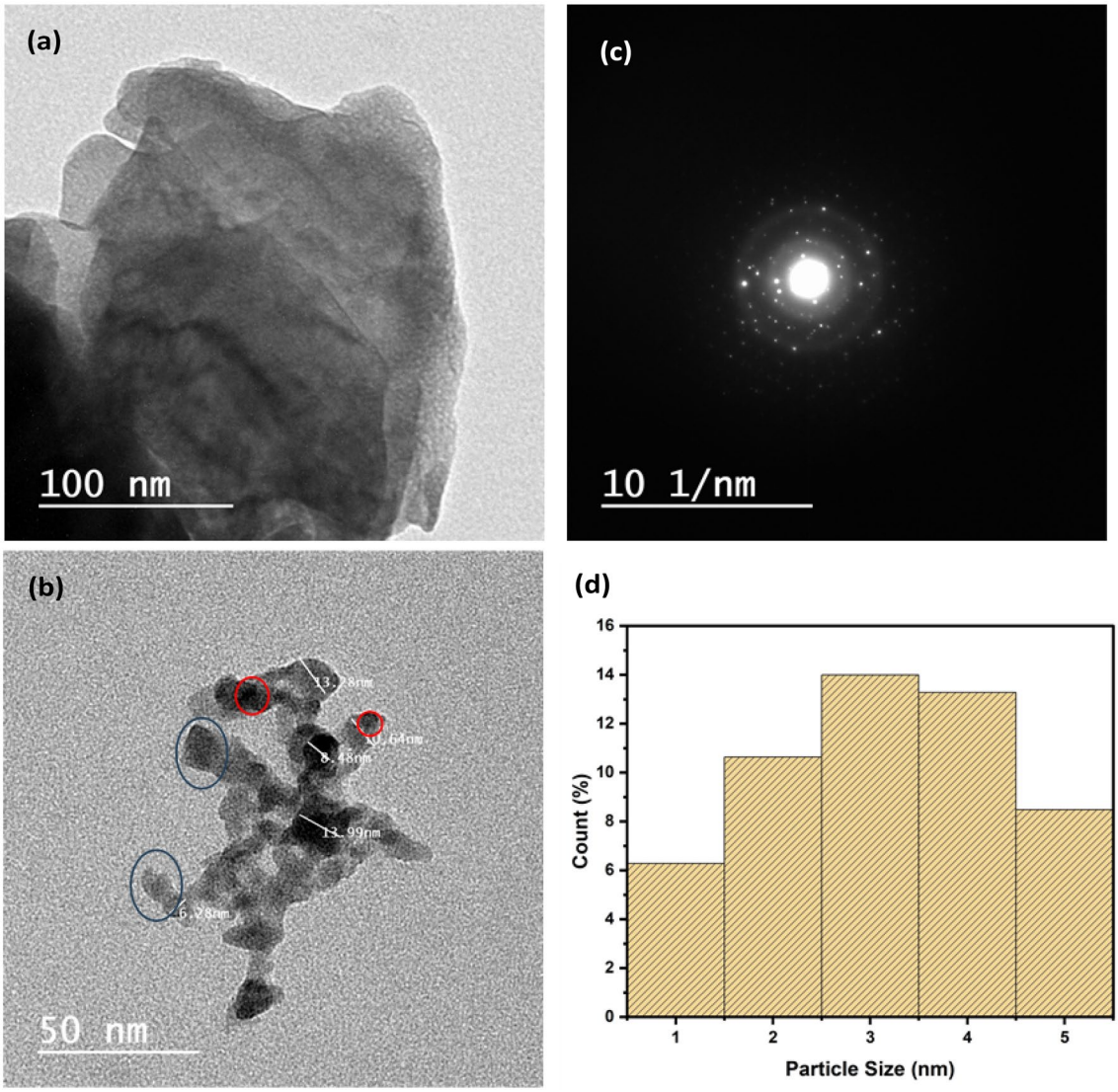

Figure 3. TEM micrographs of (**a**) Pure Nd_2O_3 NPs, (**b**) Ag/Nd_2O_3NPs, (**c**) saed pattern for Ag/Nd_2O_3NPs, (**d**) particle size histogram of Ag/Nd_2O_3NPs.

as obtained in Fig. 5[17]. In conclusion, crystallinity, and ROS generation noticeably persuade the surface area, number of active sites, and decline in the particle size that enhances dye decomposition.

The process of degrading MB dye by photocatalysis using Ag/Nd_2O_3 nanocomposite consists of many sequential stages: The photocatalytic process starts upon light absorption by the Ag/Nd_2O_3 nanocomposite, resulting in the generation of electron–hole pairs. Subsequently, the electrons that are in an excited state undergo a reaction with molecular oxygen, resulting in the formation of superoxide radicals. Simultaneously, the positively charged holes have the ability to directly oxidize the dye or water, leading to the generation of hydroxyl radicals. Subsequently, these radicals exhibit a high level of reactivity, enabling them to break down the dye molecules. Subsequently, the reactive species engage in interactions with the dye molecules, resulting in their fragmentation into smaller, less detrimental constituents[43–45]. This is the first stage at which the perceptible hue of the dye begins to diminish. Ultimately, the ideal outcome is for the dye molecules to undergo full mineralization, resulting in the formation of innocuous chemicals such as water and carbon dioxide[43–45]. The efficacy of this procedure relies on several aspects, such as the characteristics of the nanocomposite, the intensity and wavelength of the light, and the concentration of the dye1. The Ag/Nd_2O_3 nanocomposite exhibits enhanced efficacy attributed to the inclusion of silver, which facilitates light absorption and facilitates the dissociation of electron–hole pairs[46,47].

While previous research mentioned in Table 2 demonstrated significant photocatalytic activity in the removal of MB dye, the composites that were prepared did not exhibit any antibacterial properties. Additionally, the pH of the reaction was not specified in the previous studies. Furthermore, the concentration of dye used was very low. In contrast, our work investigates the photocatalytic activity using a 20 ppm dye concentration and at a pH of 6.

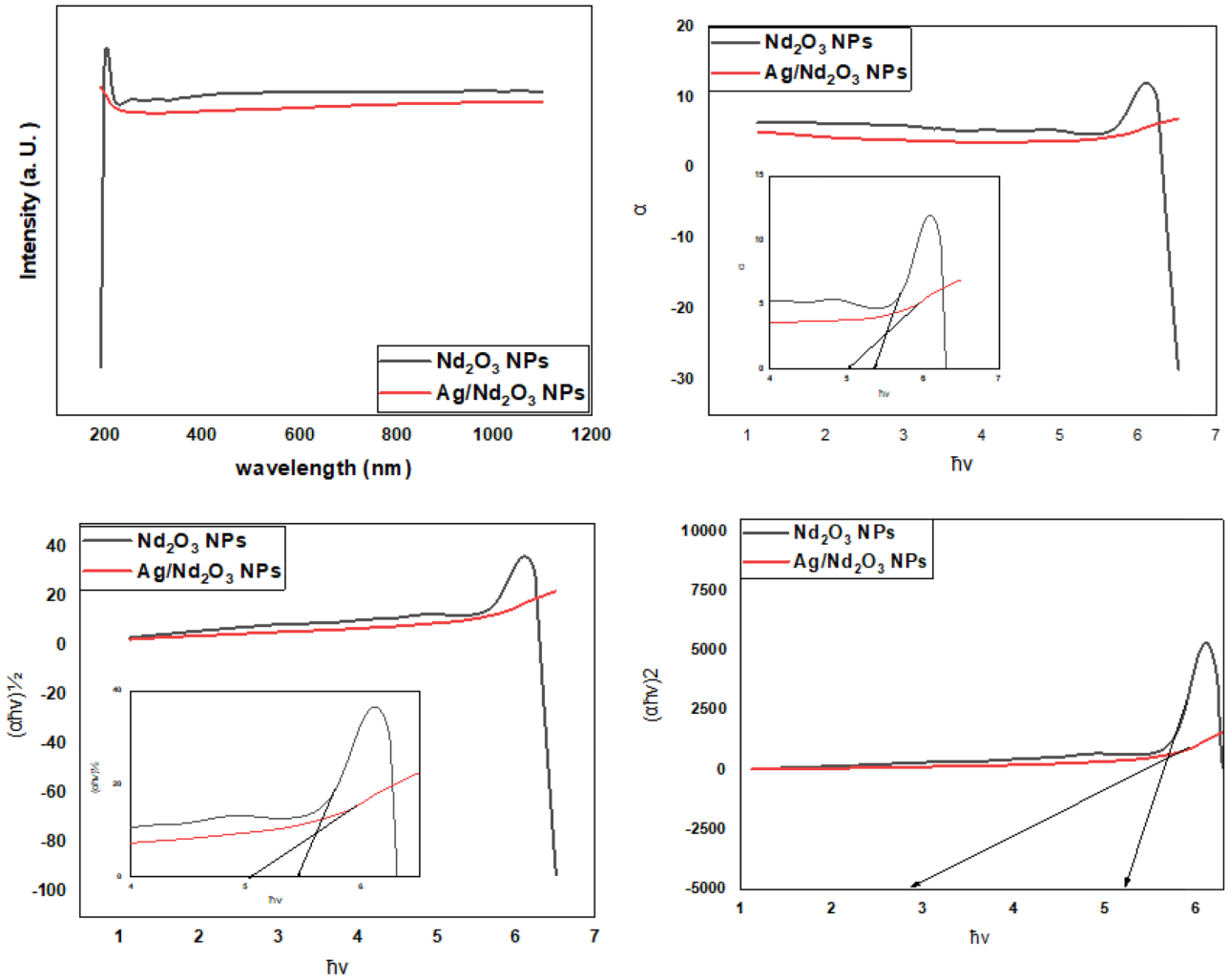

Figure 4. Optical behavior of Pure Nd_2O_3 NPs, and Ag/Nd_2O_3 NPs.

Composition	Absorption edge (eV)	Band-gap (eV)		n
		Direct	Indirect	
Nd_2O_3 NPs	6.8	6.7	5.2	1.56
Ag/Nd_2O_3 NPs	6.1	6.1	2.9	1.62

Table 1. Optical properties of Nd_2O_3 NPs and Ag/Nd_2O_3 NPs nano-composite.

Anti-bacterial activity

As *E. coli*, and *S. aureus* are the two greatest widespread bacterial species, especially after implant surgery. The introduced performance shows almost doubling an antibacterial efficiency with merging silver into pure Neodymium oxide (Nd_2O_3) nanoparticles. For illustration, as shown in Fig. 6, *S. aureus* demonstrates an inhibition zone of 9.3 ± 0.5 mm for pure Neodymium oxide (Nd_2O_3) nanoparticles (NPs), 16.7 ± 0.4 mm for Ag/Nd_2O_3 nano-composite. *E. coli* inhibition zones reveal bacterial inhibition capacity under the tested inhibitor, it shows 8.8 ± 0.4 mm for Neodymium oxide and 15.9 ± 0.3 mm for Ag/Nd_2O_3 nano-composite. The introduced antibacterial pattern is explained by the different nature of gram-positive and gram-negative bacteria, for example, *E. coli* and *S. aureus* have a divergent structure with thicker cell wall peptidoglycan layer in gram-positive than that of the gram-negative species[54]. Derakhshi et al.[55] point to the active antibacterial role of silver nanoparticles in gram-negative bacteria with 800 µg/mL. Additionally, antibacterial composite amount and nature affect the subsequent results. The introduced germicidal valuation is performed in dark, neglecting the plasmonic effect of Ag–NPs. Likewise, The mechanism of antimicrobial activity upon using silver NPs has involved the interaction of silver ions with thiol groups in pathogenic enzymes and proteins, resulting in cell death[56]. Additionally, the effectiveness of released reactive oxy-Species is affected by the inserted silver quantity, size, and distribution[57]. Further, the released oxonium ions (H_3O^+) from Nd_2O_3 mineral trioxide interrupt the cellular pH, thus bacterial

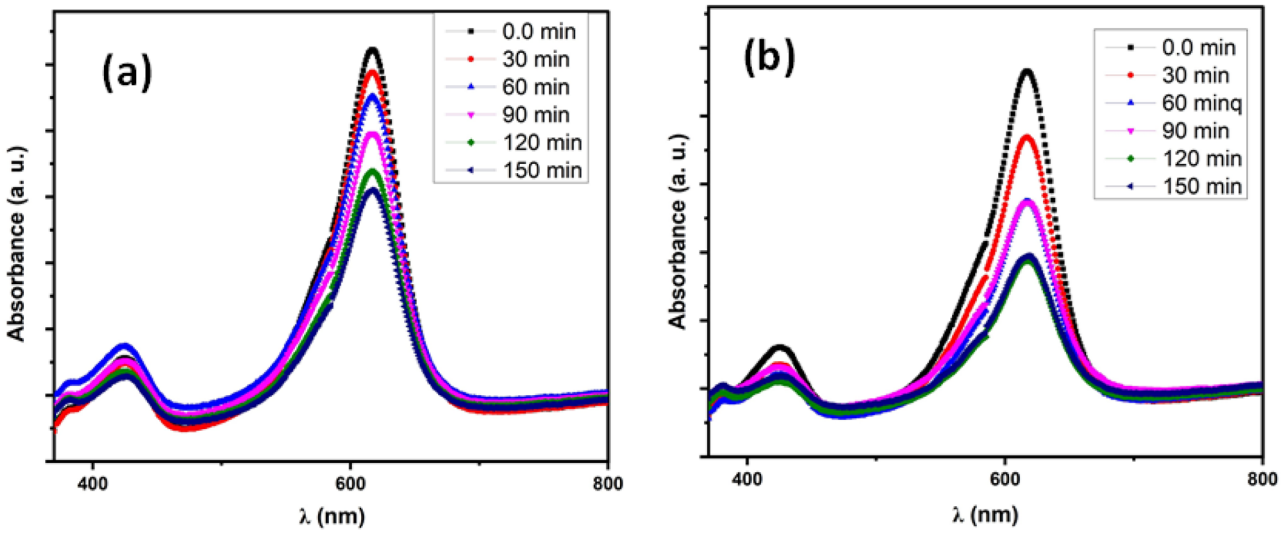

Figure 5. The degradation of MB using (**a**) pristine Nd_2O_3 NPs, (**b**) Ag/Nd_2O_3NPs.

Catalyst	Dye degradation	ppm	Time (min)	Refs.
NiCuMoO/rGO	99.2%, MB	10 ppm	80	[48]
$LaNdZr_2O_7$/SnSe	97%, Congo red	–	120	[49]
$Zn_{0.9}Ho_{0.05}M_{0.05}O$	99.7% MB and 84% MO	5 ppm	60	[50]
NiYHoO	99% MR	5 ppm	60	[51]
NiO–CdO–ZnO	99% for RhB and 98% for MB	5 ppm	60 and 90	[52]
ZnO–CoTe	98.5% MR and 99.8% MB	–	60	[53]

Table 2. comparison from different studies about the removal efficiency of different dyes.

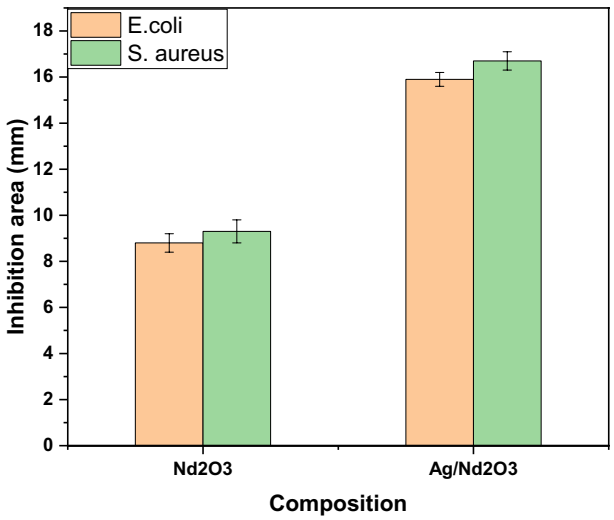

Figure 6. Antibacterial behavior of Pure Nd_2O_3 NPs, and Ag/Nd_2O_3NPs.

reproduction is disturbed, also does not allow drug-resistant phenomenon occurrence[58]. As well, Wang et al.[59] studied mineral trioxide/silver nanoparticles nano-composite, finding significant performance of La_2O_3 or Ag–La_2O_3 nanoparticles in inhibiting *E. coli* and *S. aureus* growth. Therefore, nanomaterials specially mixed systems are highly recommended for biological applications. Nd_2O_3 nanoparticles have many mechanisms by which they might impact microorganisms. To begin with, they may cause modifications in the bacterial community's composition by changing the prevalence of uncommon and delicate taxa, therefore reducing the overall effectiveness of the community. In addition, Nd_2O_3 nanoparticles have the ability to connect with the cell wall

of bacteria, especially in Gram-positive bacteria that have a thick peptidoglycan layer[60–63]. This interaction has an impact on the integrity and function of the cell wall. Nano-Nd_2O_3 may disrupt enzyme activity, specifically affecting enzymes that are essential for soil carbon and nitrogen cycle[60]. These enzymes are critical for bacterial survival and function. In addition, like other metal oxide nanoparticles, Nd_2O_3 nanoparticles has the capability to produce reactive oxygen species (ROS), which may induce oxidative stress in bacterial cells. Oxidative stress may lead to the impairment of vital cellular molecules and ultimately cause cellular demise[64]. Moreover, upon contact with bacterial cells, the nanocomposite liberates silver ions (Ag_+), which interfere with the integrity of the cell membrane, eventually leading to the demise of the cells[61,65–67]. The Nd_2O_3 nanocomposite exhibits antibacterial characteristics due to the synergistic effects of these coupled processes.

Conclusion

Structural, and compositional study of pure Neodymium oxide (Nd_2O_3 NPs), and Silver (Ag)/Neodymium oxide (Nd_2O_3) nano-composite, using XRD, FTIR, and TEM techniques. This study emphasizes optical behavior, MB dye degradation potential of pure Nd_2O_3 NPs, and (Ag/Nd_2O_3) nano-composite, alongside revealing their antibacterial performance of silver and trioxide mineral interaction with bacterial species. For instance, *S. aureus*, and *E. coli* enlargement of inhibition zone under Ag NPs insertion. *S. aureus* inhibition zone broadened from 9.3 ± 0.5 mm for pure Nd_2O_3 to 16.7 ± 0.4 mm for Ag/Nd_2O_3 composition, while *E. coli* inhibition zones extended from 8.8 ± 0.4 mm for Neodymium oxide to15.9 ± 0.3 mm for Ag/Nd_2O_3. Also, optical behavior displays band-gap contraction with assimilation with Ag NPs, which improves electronic localization. That direct and indirect transitions dropped from (6.7 to 6.1) and (5.2 to 2.9 e.V), respectively. Concerning the methylene blue degradation, Ag/Nd_2O_3 shows more efficient Methylene blue degradation than pure Nd_2O_3 in that the MB concentration dropped to almost 50% of its starting point after 150 min, while pure Nd_2O_3 reached 33% after 150 min of light irradiation. On the other hand, TEM displays the studied compositions microstructures confirming the good distribution of Ag NPs (average size 9.2 nm) upon Nd_2O_3. The results interpretations boost usage of such composites in sensors industries, and water treatment. The research team highlights the significance of investigating the prolonged stability and resilience of the Ag/Nd_2O_3 nano-composite under actual environmental conditions. Assessing the material's performance under various environmental conditions, such as temperature, pH, and humidity, would provide useful insights for its practical utilization. Moreover, the authors propose investigating the potential of the Ag/Nd_2O_3 nano-composite in other domains apart from antibacterial applications. For example, exploring its photocatalytic qualities for water treatment or its sensing capabilities for environmental monitoring might provide new opportunities for its use in these domains.

Data availability

The datasets used and/or analysed during the current study available from the corresponding author on reasonable request.

Received: 6 August 2023; Accepted: 15 March 2024
Published online: 30 April 2024

References

1. Durmus, Z., Kurt, B. Z. & Durmus, A. Synthesis and characterization of graphene oxide/zinc oxide (GO/ZnO) nanocomposite and its utilization for photocatalytic degradation of basic fuchsin dye. *ChemistrySelect* **4**(1), 271–278 (2019).
2. Mahmoudian, M. H. *et al.* Statistical modeling and optimization of dexamethasone adsorption from aqueous solution by Fe_3O_4@NH_2-MIL88B nanorods: Isotherm, kinetics, and thermodynamic. *Environ. Res.* **236**, 116773 (2023).
3. Sheikhmohammadi, A. *et al.* Fabrication of magnetic graphene oxide nanocomposites functionalized with a novel chelating ligand for the removal of Cr (VI): Modeling, optimization, and adsorption studies. *Desalin. Water Treat* **160**, 297–307 (2019).
4. Bonyadi, Z. *et al.* Biomass-derived porous aminated graphitic nanosheets for removal of the pharmaceutical metronidazole: Optimization of physicochemical features and exploration of process mechanisms. *Colloids Surf. A Physicochem. Eng. Asp.* **611**, 125791 (2021).
5. Munawar, T., Yasmeen, S., Hussain, A., Akram, M. & Iqbal, F. Novel direct dual-Z-scheme ZnO-Er_2O_3-Yb_2O_3 heterostructured nanocomposite with superior photocatalytic and antibacterial activity. *Mater. Lett.* **264**, 127357 (2020).
6. Munawar, T. *et al.* Sunlight-induced photocatalytic degradation of various dyes and bacterial inactivation using CuO–MgO–ZnO nanocomposite. *Environ. Sci. Pollut. Res.* **28**(31), 42243–42260 (2021).
7. Gola, D. *et al.* Silver nanoparticles for enhanced dye degradation. *Curr. Res. Green Sustain. Chem.* **4**, 100132 (2021).
8. Natarajan, H. C. B. S. & Tayade, R. J. Recent advances based on the synergetic effect of adsorption for removal of dyes from waste water using photocatalytic process. *J. Environ. Sci.* **65**(201), 222 (2018).
9. Karthik, C., Swathi, N. & Caroline, D. g, Green synthesized rGO-AgNP hybrid nanocomposite – An effective antibacterial adsorbent for photocatalytic removal of DB-14 dye from aqueous solution. *J. Environ. Chem. Eng.* **8**(1), 103577 (2020).
10. Dariani, R. S., Esmaeili, A., Mortezaali, A. & Dehghanpour, S. Photocatalytic reaction and degradation of methylene blue on TiO2 nano-sized particles. *Optik* **127**(18), 7143–7154 (2016).
11. Saravanan, R., Shankar, H., Prakash, T., Narayanan, V. & Stephen, A. ZnO/CdO composite nanorods for photocatalytic degradation of methylene blue under visible light. *Mater. Chem. Phys.* **125**(1–2), 277–280 (2011).
12. Natarajan, S., Bajaj, H. C. & Tayade, R. J. Recent advances based on the synergetic effect of adsorption for removal of dyes from waste water using photocatalytic process. *J. Environ. Sci. (China)* **65**, 201–222 (2018).
13. Sarojini, P. *et al.* Design of V2O5 blocks decorated with garlic peel biochar nanoparticles: A sustainable catalyst for the degradation of methyl orange and its antioxidant activity. *Materials* **16**(17), 5800 (2023).
14. Arunpandian, M., Selvakumar, K., Nagarajan, E. R. & Arunachalam, S. Ag/Nd_2o3-Zno nanocomposite: Visible active efficient photocatalytic degradation of methylene blue and its antibacterial activity. *Int. J. Innov. Technol. Explor. Eng.* **9**(22), 743–747 (2019).
15. Munawar, T. *et al.* Novel direct dual-Z-scheme ZnO-Er_2O_3-Nd_2O_3@reduced graphene oxide heterostructured nanocomposite: Synthesis, characterization and superior antibacterial and photocatalytic activity. *Mater. Chem. Phys.* **253**, 123249 (2020).
16. Tan, Y. *et al.* Neodymium oxide (Nd_2O_3) coupled tubular g-C_3N_4, an efficient dual-function catalyst for photocatalytic hydrogen production and NO removal. *Sci. Total Environ.* **773**, 145583 (2021).

17. Casillas, J. E. *et al.* Photocatalytic degradation of diclofenac using Al_2O_3-Nd_2O_3 binary oxides prepared by the sol-gel method. *Materials* **13**(6), 1345 (2020).
18. El-Sayed, F. *et al.* The photocatalytic performance of Nd_2O_3 doped CuO nanoparticles with enhanced methylene blue degradation: Synthesis. *Charact. Comp. Study* **12**(7), 1060 (2022).
19. Samson, O., Adeeko, T. O. & Makama, E. K. Synthesis and optical characterization of silver nanoparticles (Ag-NPs) thin films (TFs) prepared by silar technique. *Int. J. Curr. Res. Acad. Rev.* **5**(12), 15–24 (2017).
20. Sen, P. *et al.* Advancements in doping strategies for enhanced photocatalysts and adsorbents in environmental remediation. *Technologies* **11**(5), 144 (2023).
21. Li, H. *et al.* Effect of configuration on the photocatalytic activity of AgNPs–TiO_2 system. *Plasmonics* **13**(6), 2345–2351 (2018).
22. Nachimuthu, S. *et al.* Lawsonia inermis mediated synthesis of ZnO/Fe_2O_3 nanorods for photocatalysis – Biological treatment for the enhanced effluent treatment, antibacterial and antioxidant activities. *Chem. Phys. Lett.* **804**, 139907 (2022).
23. Nguyen, T. T. H., Kim, Y. H. & Lee, M. S. Selective dissolution of Nd_2O_3 from the mixture with Fe_2O_3 and Ga_2O_3 by using inorganic acid solutions containing ethylene glycol. *Metals* **12**(8), 1268 (2022).
24. Mukherjee, A., Van Dyck, J., Blanpain, B. & Guo, M. CSLM study on the interaction of Nd_2O_3 with $CaCl_2$ and CaF_2–LiF molten melts. *J. Mater. Sci.* **52**(3), 1717–1726 (2017).
25. Mohammadi, N., Khani, H., Gupta, V. K., Amereh, E. & Agarwal, S. Adsorption process of methyl orange dye onto mesoporous carbon material-kinetic and thermodynamic studies. *J Colloid Interface Sci.* **362**(2), 457–462 (2011).
26. Priya, B., Gupta, V. K., Pathania, D. & Singha, A. S. Synthesis, characterization and antibacterial activity of biodegradable starch/PVA composite films reinforced with cellulosic fibre. *Carbohydr. Polym.* **109**, 171–179 (2014).
27. Saravanan, R. *et al.* ZnO/Ag/CdO nanocomposite for visible light-induced photocatalytic degradation of industrial textile effluents. *J Colloid Interface Sci.* **452**, 126–133 (2015).
28. Saravanan, R., Thirumal, E., Gupta, V. K., Narayanan, V. & Stephen, A. The photocatalytic activity of ZnO prepared by simple thermal decomposition method at various temperatures. *J. Mol. Liq.* **177**, 394–401 (2013).
29. Jehinder, J. & Umadevi, M. Synthesis and characterization of monodispersed silver nanoparticles. *Adv. Nat. Sci. Nanosci. Nanotechnol.* **3**, 035013 (2012).
30. Rahman, M. M., Wahid, A., Alam, M. M. & Asiri, A. M. Efficient 4-nitrophenol sensor development based on facile Ag@Nd_2O_3 nanoparticles. *Mater. Today Commun.* **16**, 307–313 (2018).
31. Zhang, X. & Hao, L. Preparation and catalytic activity of M_2O_3/CNTs (M = Y, Nd, Sm) nanocomposites by solvothermal process. *J. Nanomater.* **2018**, 1–8 (2018).
32. Keikhaei, M., Motevalizadeh, L. & Attaran-Kakhki, E. Optical properties of neodymium oxide nanoparticle-doped polyvinyl alcohol film. *Int. J. Nanosci.* **15**(04), 1650012 (2016).
33. Shimpi, N. G., Khan, M., Shirole, S. & Sonawane, S. Process optimization for the synthesis of silver (AgNPs), iron oxide (α-Fe_2O_3NPs) and core-shell (Ag-Fe_2O_3CNPs) nanoparticles using the aqueous extract of alstonia scholaris: A greener approach. *Open Mater. Sci. J.* **12**(1), 29–39 (2018).
34. Dawy, M., Rifaat, H. M. & Menazea, A. A. Characterization of ag nanoparticles by nanosecond pulsed laser ablation doped in chitosan. *Curr. Sci. Int.* **4**(4), 6 (2015).
35. Jouyban, A. & Rahimpour, E. Optical sensors based on silver nanoparticles for determination of pharmaceuticals: An overview of advances in the last decade. *Talanta* **217**, 121071 (2020).
36. Menazea, A. A., Awwad, N. S., Ibrahium, H. A. & Ahmed, M. K. Casted polymeric blends of carboxymethyl cellulose/polyvinyl alcohol doped with gold nanoparticles via pulsed laser ablation technique; morphological features, optical and electrical investigation. *Radiat. Phys. Chem.* **177**, 109155 (2020).
37. Menazea, A. A. One-pot pulsed laser ablation route assisted copper oxide nanoparticles doped in PEO/PVP blend for the electrical conductivity enhancement. *J. Mater. Res. Technol.* **9**(2), 2412–2422 (2020).
38. El-dek, S. I., Mansour, S. F., Ahmed, M. A. & Ahmed, M. K. Microstructural features of flower like Fe brushite. *Prog. Nat. Sci. Mater. Int.* **27**(4), 520–526 (2017).
39. Mansour, S. F., El-dek, S. I., Ahmed, M. A., Abd-Elwahab, S. M. & Ahmed, M. K. Effect of preparation conditions on the nanostructure of hydroxyapatite and brushite phases. *Appl. Nanosci.* **6**, 991–1000 (2016).
40. Ahmed, M. A., Mansour, S. F., El-dek, S. I., Abd-Elwahab, S. M. & Ahmed, M. K. Characterization and annealing performance of calcium phosphate nanoparticles synthesized by co-precipitation method. *Ceram. Int.* **40**(8), 12807–12820 (2014).
41. Zuo, R. *et al.* Photocatalytic degradation of methylene blue using TiO_2 impregnated diatomite. *Adv. Mater. Sci. Eng.* **2014**, 1–7 (2014).
42. Chakhtouna, H., Benzeid, H., Zari, N., Qaiss, A. E. K. & Bouhfid, R. Recent progress on Ag/TiO_2 photocatalysts: Photocatalytic and bactericidal behaviors. *Environ. Sci. Pollut. Res. Int.l* **28**(33), 44638–44666 (2021).
43. Naggar, A. H. *et al.* Morphological dependence of metal oxide photocatalysts for dye degradation. *Inorganics* **11**(12), 484 (2023).
44. Kannan, K. *et al.* Facile fabrication of novel ceria-based nanocomposite (CYO-CSO) via co-precipitation: Electrochemical, photocatalytic and antibacterial performances. *J. Mol. Struct.* **1256**, 132519 (2022).
45. Sa-nguanprang, S., Phuruangrat, A., Karthik, K., Thongtem, S. & Thongtem, T. Tartaric acid-assisted precipitation of visible light-driven Ce-doped ZnO nanoparticles used for photodegradation of methylene blue. *J. Aust. Ceram. Soc.* **56**(3), 1029–1041 (2020).
46. Nagajyothi, P. C. *et al.* Environmentally friendly synthesis: Photocatalytic dye degradation and bacteria inactivation using Ag/f-MWCNTs composite. *J. Cluster Sci.* **32**(3), 711–718 (2021).
47. Boutalbi, A. *et al.* Photocatalytic dye degradation efficiency and reusability of potassium polyacrylate hydrogel loaded Ag@ZnO nanocomposite. *Transit. Met. Chem.* **48**(5), 353–363 (2023).
48. Areej, F. *et al.* Synthesis and characterization of rGO-supported Mo/Cu dual-doped NiO nanocomposite for the elimination of dye pollutant. *Appl. Nanosci.* **13**(8), 5641–5657 (2023).
49. Gohar, R. S. *et al.* Hydrothermal preparation of LaNdZr2O7 – SnSe nanocomposite for electrochemical supercapacitor and degradation of contaminants' applications. *J. Energy Storage* **52**, 104930 (2022).
50. Nadeem, M. S. *et al.* Facile synthesis of sunlight driven photocatalysts Zn0.9Ho0.05M0.05O (M = Pr, Sm, Er) for the removal of synthetic dyes from wastewater. *Surf. Interfaces* **34**, 102376 (2022).
51. Munawar, T. *et al.* Tunability of physical properties of NiO by the introduction of rare earth metal (Y, Ho) dual doping for natural sunlight-driven photocatalysis. *J. Mater. Sci. Mater. Electron.* **34**(7), 687 (2023).
52. Munawar, T., Iqbal, F., Yasmeen, S., Mahmood, K. & Hussain, A. Multi metal oxide NiO–CdO–ZnO nanocomposite–synthesis, structural, optical, electrical properties and enhanced sunlight driven photocatalytic activity. *Ceram. Int.* **46**(2), 2421–2437 (2020).
53. Alharbi, F. F. *et al.* Sunlight activated S-scheme ZnO–CoTe binary photocatalyst for effective degradation of dye pollutants from wastewater. *Surf. Interfaces* **31**, 101991 (2022).
54. Xu, J. *et al.* Influence of Ag alloying on the antibacterial properties, bio-corrosion resistance and biocompatibility of α-Nb_5Si_3 nanocrystalline coating. *Appl. Surf. Sci.* **503**, 144082 (2020).
55. Derakhshi, M., Ashkarran, A. A., Bahari, A. & Bonakdar, S. Shape selective silver nanostructures decorated amine-functionalized graphene: A promising antibacterial platform. *Colloids Surf. A Physicochem. Eng. Asp.* **545**, 101–109 (2018).
56. Loiseau, A. *et al.* Silver-based plasmonic nanoparticles for and their use in biosensing. *Biosensors* **9**(2), 78 (2019).
57. Xie, Y. Y. *et al.* Development and antibacterial activities of bacterial cellulose/graphene oxide-CuO nanocomposite films. *Carbohydr Polym* **229**, 115456 (2020).

58. Zhao, Y., Xu, J., Li, Z., Fu, T. & Jiang, S. In vitro antibacterial properties of $MoO_3/SiO_2/Ag_2O$ nanocomposite coating prepared by double cathode glow discharge technique. *Surf. Coat. Technol.* **397**, 125992 (2020).
59. Wang, K. *et al.* A hybrid antioxidizing and antibacterial material based on Ag-La_2O_3 nanocomposites. *J. Inorg. Biochem.* **141**, 36–42 (2014).
60. Xu, Y. *et al.* Nano-Nd_2O_3 reduced soil bacterial community function by altering the relative abundance of rare and sensitive taxa. *Environ. Sci. Pollut. Res.* **30**(32), 78332–78338 (2023).
61. Rangayasami, A., Kannan, K., Joshi, S. & Subban, M. Bioengineered silver nanoparticles using *Elytraria acaulis* (L.f.) Lindau leaf extract and its biological applications. *Biocatal. Agric. Biotechnol.* **27**, 101690 (2020).
62. Surendran, P. *et al.* Fluorescent carbon quantum dots from Ananas comosus waste peels: A promising material for NLO behaviour, antibacterial, and antioxidant activities. *Inorg. Chem. Commun.* **124**, 108397 (2021).
63. Kannan, K., Radhika, D., Gnanasangeetha, D., Krishna, L. S. & Gurushankar, K. Y^{3+} and Sm^{3+} co-doped mixed metal oxide nanocomposite: Structural, electrochemical, photocatalytic, and antibacterial properties. *Appl. Surf. Sci. Adv.* **4**, 100085 (2021).
64. Al-Fakeh, M. S. & Al-Otaibi, N. F. Nd_2O_3, Cr_2O_3, and V_2O_3 nanoparticles via calcination: Synthesis, characterization, antimicrobial and antioxidant activities. *J. Nanotechnol.* **2022**, 7794939 (2022).
65. Cuadra, J. G. *et al.* ZnO/Ag nanocomposites with enhanced antimicrobial activity. *Appl. Sci.* **12**(10), 5023 (2022).
66. Bai, X. *et al.* Photocatalytic degradation of some typical antibiotics: Recent advances and future outlooks. *Int. J. Mol. Sci.* **23**(15), 8130 (2022).
67. Chinnaiah, K. *et al.* Ag nanoparticles synthesized by *Datura metel* L. Leaf extract and their charge density distribution, electrochemical and biological performance. *Chem. Phys. Lett.* **807**, 140083 (2022).

Acknowledgements

The authors extend their appreciation to the Ministry of Education in KSA for funding this research work through the project number KKUIFP2- DA-8.

Author contributions

M.T.E. Investigation, Writing—Review and Editing. M.A.E.-M. Investigation, Writing—Review and Editing. N.S.A. Investigation, Writing—Review and Editing. H.A.I. Investigation, Writing—Review and Editing. A.A.M. Methodology, Formal analysis, Investigation, Writing—Original Draft, Writing—Review and Editing.

Competing interests

The authors declare no competing interests.

Additional information

Correspondence and requests for materials should be addressed to A.A.M.

Reprints and permissions information is available at www.nature.com/reprints.

Publisher's note Springer Nature remains neutral with regard to jurisdictional claims in published maps and institutional affiliations.